The Design and Fabrication of Microdisk Resonators for Terahertz Frequency Operation

T. N. Adam, S. Shi, S. K. Ray, R. T. Troeger, D. Prather, and J. Kolodzey
Department of Electrical and Computer Engineering
University of Delaware
Newark, DE 19716, USA
http://www.ee.udel.edu/~kolodzey

Abstract

The design and fabrication of resonators and waveguides operating at THz frequencies are reported. Resonance frequencies, mode confinement, quality factors, and stop-bands were calculated for resonators with and without photonic elements. The estimations show that very narrow modes can exist within the propagation bandgap of a photonic lattice. Microdisk devices were designed and fabricated for high-quality whispering-gallery modes centered around 10 THz. Combined with silicon-germanium quantum wells grown by molecular beam epitaxy, these resonators are promising candidates for silicon-based miniature far-infrared lasers.

Introduction

Strong molecular absorption of terahertz radiation (1-30 THz) due to vibrational and rotational transitions[1] makes THz optical components and devices an attractive choice for chemical and biological sensing and imaging applications[2]. The predicted low absorption coefficient of electromagnetic radiation at 30 THz in air suggests a wide range of free-space communication[3] and military applications, such as ranging[4] and imaging[5]. Outside this atmospheric window, the extremely high absorption coefficient ($>10^3$ dB/km), makes it suitable for short-range applications. Compared to microwave systems, THz-based devices are expected to be smaller and more compact due to the shorter wavelength. To support new applications in this frequency regime, components such as sources, detectors, and couplers must be designed and optimized. Our sources and detectors are based on intersubband transitions in SiGe quantum wells[6]. The resonators and waveguides are based on structures that incorporate photonic crystal elements for frequency selection and mode control. Microdisk resonators support high azimuthal whispering gallery modes with quality factors near 10^5, and are therefore superb candidates for ultra-low-threshold lasers. To fabricate THz microdisks that can be integrated with quantum wells and photonic crystal elements, we have developed an anisotropic deep reactive ion etching technique that combines sacrificial micromasking layers with cyclical replenishing and removal. This technique has led to the fabrication of unique resonator and waveguide structures that will be described here.

Theory

Dielectric resonators[7] and waveguides with photonic crystal elements were simulated using the Finite-Difference Time-Domain (FDTD) method. Our mathematical model and numerical method are published elsewhere[8]. Briefly, the structures were meshed in two dimensions, using a perfectly matched layer as the absorbing boundary and a $\lambda/40$ sampling grid, where λ is the center wavelength (30μm or 10 THz). After launching a Gaussian pulse having a 1/e bandwidth spanning the frequency range of interest (here $\pm$ 5 THz), the electric and magnetic field components were calculated and stored at a time interval of $\Delta t = \Delta/2c_0$, where c_0 is the velocity of light in free-space and Δ is the sampling grid step size. After N time steps, the computation was ended and field components were Fourier transformed with a frequency resolution of $\Delta f = 1/N\Delta t$.

Simulations were performed for a microring structure suspended in air with an inner radius of 70 μm, annulus width of 8 μm, with and without photonic crystals (PC) of varying period and size. As shown in Figure 1(a), the microring permits the propagation of a multitude of frequencies without any PC. The most effective stop-band was achieved using etched holes with a radius of 2.5 μm and period of 7.97 μm. In this configuration, which is displayed in Figure 1(b), the propagation of light with frequencies between 8 and 11.5 THz was forbidden. When every fourth element in the photonic crystal was omitted, a very narrow mode around 9.55 THz within the forbidden gap was allowed, depicted in Figure 1(c). The best transmission properties of this frequency were achieved by adjusting the ring radius and PC period to 70.2 and 8 μm, respectively.

Microdisk resonators supported by a pedestal have been predicted to exhibit quality factors in excess of 5,000[7]. We propose to combine the high-quality factor and mode confinement of microdisks with the propagation selectivity of PCs to select the highest quality modes in microdisk resonators.

Experimental

Optical components, such as waveguides and resonators, often require extremely low surface roughness and high aspect ratios (HAR) to sustain the predicted propagation properties. We have developed and optimized a novel two-part etching process that produces freestanding HAR features in silicon grown by chemical vapor deposition (CVD) on highly doped silicon substrates. The process is schematically shown in Figure 2. Lightly doped layers (approximately 140 Ωcm) were grown by atmospheric-pressure chemical-vapor deposition (APCVD) on p-type $5 \cdot 10^{18} cm^{-3}$ doped three-inch silicon substrates using dichlorosilane as the precursor and hydrogen as carrier gas. After a short cleaning etch in hydrochloric acid vapor, the layers were deposited at a substrate temperature of 1100 °C. No dislocations were observed using Nomarski-contrast microscopy. The doping concentration was constant throughout the layer and the interface was sufficiently abrupt, as confirmed by spreading resistance measurements on a 1-degree beveled edge.
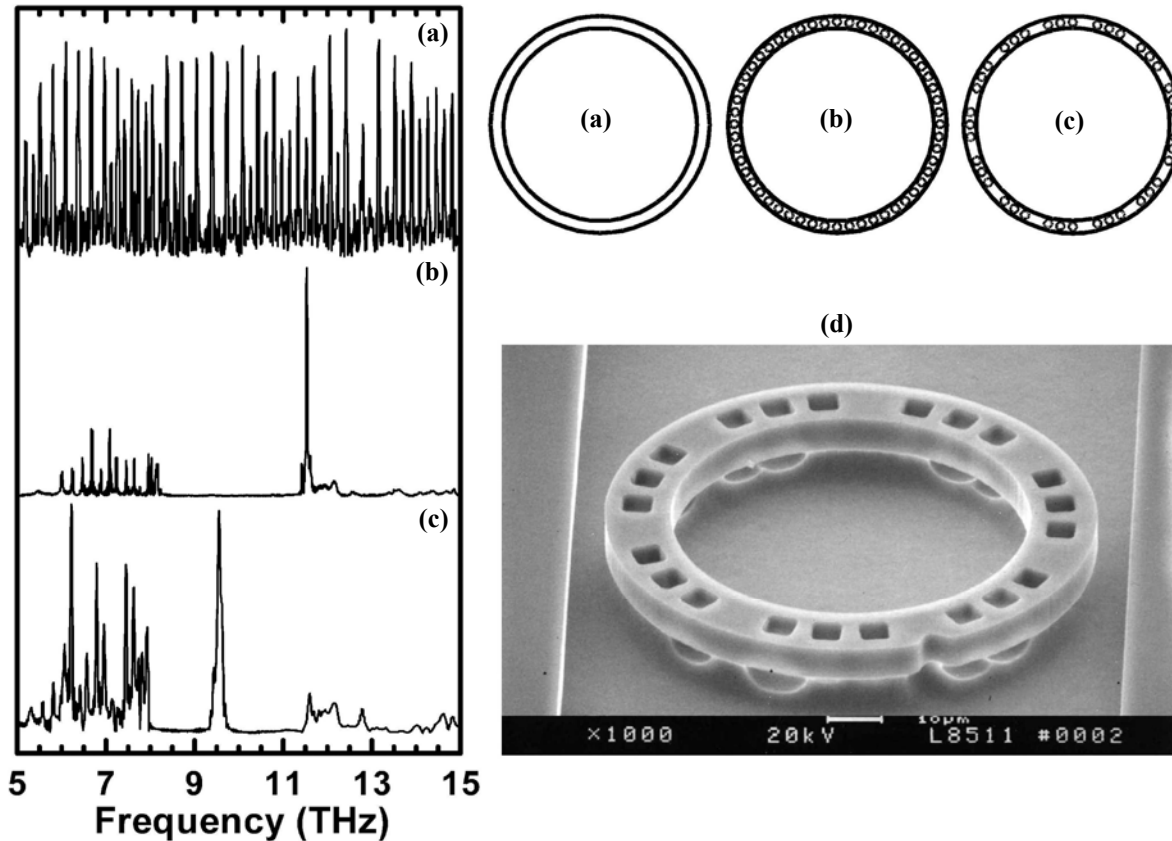
Figure 1: **Finite-Difference Time-Domain simulations of microring resonator. The ring has an inner radius of 70 μm, annulus width of 8 μm, PC period of 7.97 μm, and PC radius of 2.5 μm. (a): Ring resonator without photonic crystal structure showing broadband character. (b): Periodic PC etched into the ring, resulting in a stop-band between 8 and 11.5 THz. (c): Periodic placement of defects in PC permitting the propagation of a narrow part at 9.55 THz inside the stop-band. (d): Scanning electron micrograph of fabricated microring structure with PC and periodic defect. Linear waveguides are nearby in order to capture the evanescent tail of the propagating mode.**

Vertical Etch

Presently, high-aspect ratio features in silicon are commonly obtained in dry etchers. The silicon etching process with the highest dissolution rates and anisotropies is patented by the Robert-Bosch GmbH[9]. However, this process relies on fast gas and pressure management, helium-flow-cooled substrates, requires inductive plasma enhancement, and in its original configuration does not allow irregularly shaped samples to be processed. We have developed a similar process that operates on conventional parallel plate reactive ion etchers. This process is inherently much slower due to the lack of plasma enhancement by an inductive coil.
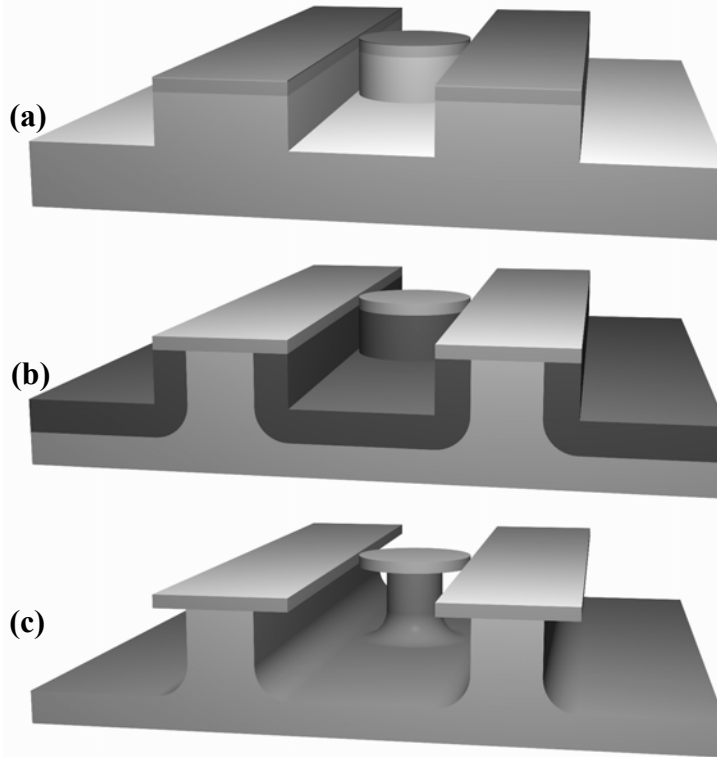
Figure 2: **Schematic Birdseye view of the process flow for freestanding all-silicon devices. The microdisks are placed near linear waveguides to capture the evanescent tail of the well-confined optical mode through optical tunneling. (a): Multi-step reactive ion etch producing nearly straight side walls, approximately 10 μm deep. (b): Formation of porous silicon in highly doped areas only. (c): Anodic oxidation and removal of porous silicon.**

Consequently, no further substrate cooling is required other than the water-cooled platen. Our system was a Plasmatherm 790 parallel plate etcher having an 8-inch substrate holder. Process gases were introduced through a bank of eight massflow controllers using a shower head distributor. A feedback-controlled flapper-type throttle valve stabilized the pressure. The 13.56 MHz rf-power was coupled to the 8-inch parallel plates with a 7-cm separation. The (typically two-step) Bosch process is incompatible with this configuration, because it does not selectively deposit the protective polymer on the vertical sidewalls of the etched structures, even at the highest rf-powers and lowest gas pressures. In addition, the horizontal coverage could not be removed during the etch part of the cycles without sufficient selectivity to photoresist. We have therefore added a third step to the cyclic process and optimized each one individually.

A schematic overview of this process is depicted in Figure 3. Positive photoresist (AZ5214E[10]) was spun coated and patterned using a contact exposure mask aligner. During the etching step, silicon was isotropically etched in a mixture of SF_6 and He optimized in power, pressure, and gas composition for maximal etch rates and mask selectivities. The lack of inductive coils required a plasma pressure of 200 mT to achieve satisfying etch rates, but
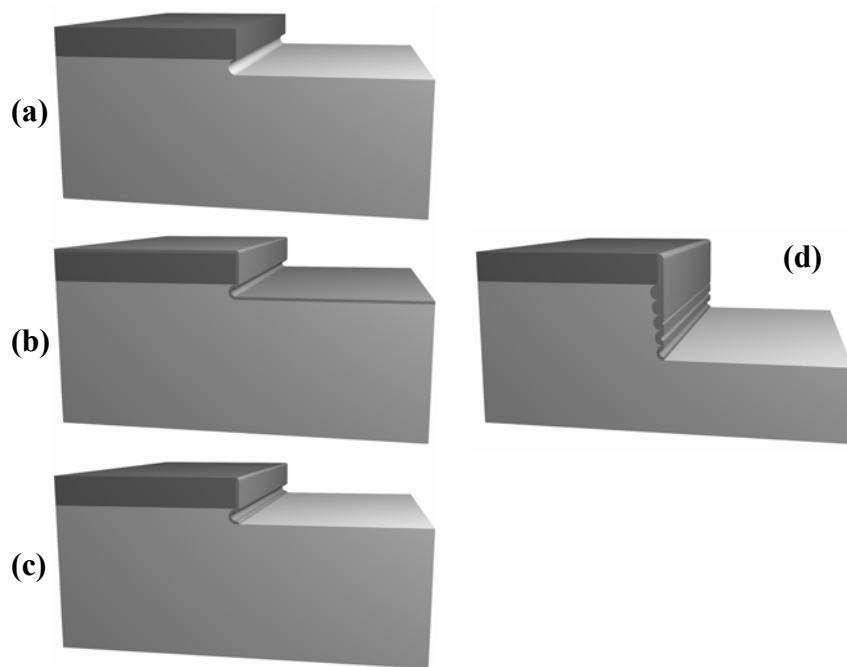
Figure 3: **Schematic Birdseye view of a feature evolving during multi-step reactive ion etch process. Substrate is silicon and masking material is photoresist. (a): Isotropic silicon etch to a typical depth of 300 nm. High pressures, low powers, and gas mixtures of SF_6 and He ensure mask selectivity and high etching rates. (b): Isotropic deposition of etch-prohibiting polymer in a mixture of CF_4 and H_2. (c): Anisotropic removal of polymer in short high-ion energy plasma. Horizontal surfaces are cleared of the polymer by ion-bombardment assisted etching. (d): Feature edge after a few cycles. Due to the accumulation of polymer towards the top of the feature the underlying silicon sidewall can never be perfectly vertical.**

decreased the lateral uniformity drastically. Polymer deposition was performed in a second step using a mixture of CF_4 and H_2 optimized for highest deposition rates. This etch-prohibiting polymer was anisotropically removed employing a short low-pressure high-energy plasma step in a mixture of SF_6 and He. The system was evacuated to <1 mT between all plasma steps, and the timing was adjusted to yield the target depth/cycle, minimal required sidewall polymer thickness, best mask selectivity, and highest aspect ratio. A depth of 10 μm was typically achieved after 8 to 10 hours of cyclic etching. Unlike a version of the Bosch process, this process did not promote forward scattering of the sidewall material, to maintain high mask selectivity. Consequently, the etch-prohibiting polymer accumulated towards the top of the features. Typically, 15 nm of polymer were required during each cycle, resulting in a total thickness of 0.5 μm after 33 cycles. The sidewall protection layer caused the features to broaden at the bottom, producing an aspect ratio of ≈20.

Porous Silicon Formation and Removal

Preliminary investigations revealed that traditional doping-selective etchants, such as HF:HNO$_3$:CH$_3$COOH (1:3:8) do not provide sufficient selectivities to allow micron and submicron features to be fabricated. Even after extensive optimization, a doping contrast of $\approx$ 5·10^{18}cm^{-3}/10^{14}cm^{-3} = 50,000 only produced a selectivity of less than 20. While electrochemical etching or polishing is theoretically capable of stopping at low-doped or undoped layers, the selectivity degenerates when the stopping layer and its features are exposed during the bulk removal. In a typical electrochemical setup, the epitaxial layer is covered with wax while the bulk is removed from the backside. However, we observed excellent selectivities for porous silicon formation at lower current densities. Unprotected features were subjected current densities of less than 10 mA/cm^2 in 49 % HF. The underlying p^{++} layer was converted to porous silicon, subsequently oxidized anodically in KNO$_3$, and removed in ethanoic HF. A final short dip in 1% KOH removed remaining porous silicon debris, as still visible on the left-hand side of Figure 4. Freestanding waveguide samples were stored in isopropanol and dried in a CO$_2$ critical-point dryer, while microdisk samples were rinsed in isopropanol and allowed to dry in air.

This process was used to fabricate linear waveguides, microrings, and microdisks as displayed in Figure 1(d) and Figure 4, to serve as THz resonators. The resonators and photonic crystal elements were patterned and etched using one photoresist masking layer. The structures were anisotropically etched with 300 nm per cycle to a depth of 10 μm. Microrings were subsequently undercut 3 μm while microdisk were underetched ≈20 μm.

Discussion of Results

We have fabricated freestanding all-silicon waveguides, couplers, and resonators with excellent surface and sidewall roughness and incorporated scale-model photonic elements, as depicted in Figure 4. The propagation of light at THz frequencies is currently under investigation using state-of-the-art Fourier Transform Infrared Spectroscopy. Transmission spectra can be recorded with resolutions as high as 0.125 cm^{-1} using a helium-cooled silicon bolometer detector and a broadband glowbar infrared source. However, coupling to and from our structures was difficult to obtain. Although optical fibers may be positioned accurately in a laboratory environment using micrometer xyz-stages, no far-infrared fibers were available to date. Most commonly, silicon or germanium lenses or prisms are employed, but the freestanding character of our structures prohibits a direct contact. Effectively, only end firing to freestanding waveguides was possible, which is expected to increase coupling losses to several tens of decibels. Until now, we were not able to couple to our structures efficiently enough to measure the transmission characteristics.

We have shown with Finite-Difference Time-Domain simulations that resonators based on whispering gallery modes are promising candidates for ultra-low threshold lasers and that holes etched periodically into our structures form photonic crystals with desirable photonic bandgap characteristics. Frequency selection using periodic defects was effective allowing narrow band propagation.
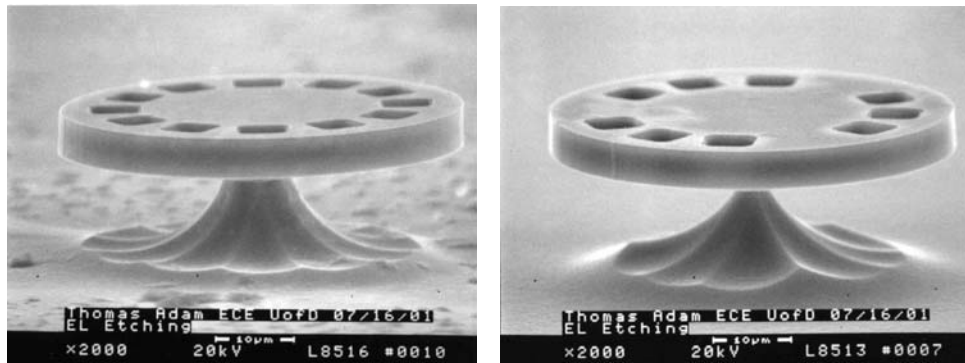
Figure 4: Birdseye view scanning electron micrograph of fabricated 50-μm diameter microdisk with photonic crystal elements. Left: Stop-band arrangement. Right: Frequency selection mode.

Acknowledgements

References

[1] R. A. Cheville, D. Grischkowski," *Observation of pure rotational spectra in the v_2 band of hot H_2O in flames*", Optics Letters **23**(07), 1 April 1998, pp. 531

[2] K. J. Siebert, H. Quast, R. Leonhardt, T. Löffler, M. Thomson, T. Bauer, H. G. Roskos, S. Czasch, "*Continuous-wave all-optoelectronic terahertz imaging*", Applied Physics Letters **80**(16), 22 April 2002, pp. 3003

[3] S. Blaser, D. Hofstetter, M. Beck, J. Faist, "*Free-space optical data link using Peltier-cooled quantum cascade laser*", Electronics Letters **37**(12), 7 June 2001, pp. 778

[4] R. A. Cheville, D. Grischkowski, "*Time domain terahertz impulse ranging studies*", Applied Physics Letters **67**(14), 2 October 1995, pp. 1960

[5] K. McClatchey, M. T. Reiten, R. A. Cheville, "*Time resolved synthetic aperture terahertz impulse imaging*", Applied Physics Letters **79**(27), 31 December 2001, pp. 4485

[6] T. N. Adam, R. T. Troeger, S. K. Ray, U. Lehmann, J. Kolodzey, "*Terahertz Emitting Devices Based on Intersubband Transitions in SiGe Quantum Wells*", Proceedings of the 10th International Symposium on Nanostructures: Physics and Technology, St. Petersburg, 17-21 June 2002, pp. 441

[7] S. Shi, D. Prather, L. Yang, J. Kolodzey, "*Influence of Support Structure on Microdisk Resonator Performance*", Optical Engineering in July, 2002, in press

[8] S. Shi, L. Yang, D. Prather, "*Numerical Study of Axisymmetric Dielectric Resonators*", IEEE Transactions on Microwave Theory and Techniques **49**(9), September 2001

[9] Robert Bosch GmbH, US Pat. 5501893, 6127273, 6214161, 6284148

[10] Clariant Corporation, 70 Meister Avenue, Somerville, NJ 08876, USA